Scientific Reports

https://doi.org/10.1038/s41598-026-47000-z

Article in Press

Synthesis and characterization of graphitic carbon nitride-doped carbon (Cu-Al/Biochar@g-C_3N_4) for quinoline yellow removal by the Fenton process: optimization by the response surface method

Received: 5 February 2026

Accepted: 28 March 2026

Published online: 04 April 2026

Cite this article as: Foko R.U.N., Mafo S.G.M., Djouda C.M.N. *et al.* Synthesis and characterization of graphitic carbon nitride-doped carbon (Cu-Al/Biochar@g-C_3N_4) for quinoline yellow removal by the Fenton process: optimization by the response surface method. *Sci Rep* (2026). https://doi.org/10.1038/s41598-026-47000-z

Roland Urselin Noumsi Foko, Sandrale Grace Mokue Mafo, Carolle Miriane Nawa Djouda, Donald Raoul Tchuifon Tchuifon, Ahmad Hosseini-Bandegharaei, Zaher Mundher Yaseen, Jiang Wu & Cyrille Ghislain Fotsop

Synthesis and characterization of graphitic carbon nitride-doped carbon (Cu-Al/Biochar@g-C_3N_4) for quinoline yellow removal by the Fenton process: Optimization by the response surface method

Roland Urselin Noumsi Foko[1], Sandrale Grace Mokue Mafo[2*], Carolle Miriane Nawa Djouda[3], Donald Raoul Tchuifon Tchuifon[3*], Ahmad Hosseini-Bandegharaei[4-6*], Zaher Mundher Yaseen[7], Jiang Wu[8], Cyrille Ghislin Fotsop[9]

[1] *Department of Chemistry, Faculty of Sciences, University of Douala, PO Box: 24157, Douala, Cameroon*
[2] *Laboratory of Process Engineering, Advanced Teacher's Training School for Technical Education, University of Douala, PO Box 1872, Douala, Cameroon*
[3] *Department of Process Engineering, Laboratory of Chemical Engineering and Industrial Bioprocesses, National Polytechnic School of Douala, University of Douala, BP 2701, Douala, Cameroon*
[4] *Faculty of Chemistry, Semnan University, Semnan, Iran*
[5] *Scientific Research Center, Al-Ayen Iraqi University (AUIQ), Nasiriyah, Thi-Qar, 64001, Iraq*
[6] *Department of Sustainable Engineering, Saveetha School of Engineering, SIMATS, Chennai, Tamil Nadu 602105, India*
[7] *Civil and Environmental Engineering Department, King Fahd University of Petroleum & Minerals, Dhahran 31261, Saudi Arabia*
[8] *College of Energy and Mechanical Engineering, Shanghai University of Electric Power, Shanghai 200090, China*
[9] *Institute of Chemistry, Faculty of Process and Systems Engineering, University Splatz 2, 39106 Magdeburg, Germany*

Correspondence: Sandrale Grace Mokue Mafo; Donald Raoul Tchuifon Tchuifon; and Ahmad Hosseini-Bandegharaei (sandralemafo@gmail.com; tchuifondonald@yahoo.fr; and ahoseinib@yahoo.com)

Abstract

This study describes the synthesis and characterization of a biochar doped with graphitic carbon nitride and modified with copper and aluminum (Cu-Al/Biochar@g-C_3N_4). This composite was developed to optimize the removal of quinoline yellow using the Fenton process and the method, employing the response surface methodology. The physicochemical characterizations, notably Fourier-transform infrared spectroscopy (FTIR), highlighted the aluminum-oxygen and copper-oxygen bonds, indicating the successful incorporation of these metals into the biochar matrix. X-ray diffraction (XRD) revealed a crystalline structure with an average grain size of 7.726 nm for the raw biochar and 16.677 nm for Cu-Al/Biochar@g-C_3N_4. The analysis also identified mineral phases such as goethite (FeO(OH)) and calcite ($CaCO_3$). The results of the BET analysis showed that the raw biochar and the Cu-Al/Biochar@g-C_3N_4 composite exhibit type IV isotherms. The modification of the raw biochar increased the specific surface area of the doped biochar by 10.52 m^2/g. Furthermore,

EDX analyses confirmed that the raw biochar is typical of pyrolyzed biochar and the efficiency of the impregnation. The influence of the composite mass, pH, and pollutant concentration during the heterogeneous Fenton process allowed us to establish an equilibrium time of 150 minutes. The optimization of the operational parameters was carried out using a Box-Behnken (BBD) design, varying three parameters: pH (2-6); [E104] (50-100 mg/l) and H_2O_2 (13-65 mM). The results obtained show a degradation percentage of 92.33% under optimal conditions with a high coefficient of determination of R^2 = 90.56% and $R^2_{adjusted}$ = 82.07%. The recovery and reusability study of the catalyst shows an efficiency after three cycles with a degradation rate of 50.28%. Mathematical modeling-based optimization showed the best conditions at pH 5, a dye concentration of 100 mg/L, a catalyst dosage of 50 mg, and an H_2O_2 concentration of 65 mM, achieving a degradation efficiency of 92.33% in 150 minutes. These results suggest that Cu-Al/Biochar@g-C_3N_4 is promising for getting rid of quinoline yellow.

Keywords : Quinoline yellow, Biochar, Advanced oxidation process, Doped composite material

Introduction

Modern human activities inevitably lead to the discharge of effluents containing various toxic chemicals into the environment [1]. These effluents are often composed of heavy metals, drug residues, and dyes, which are in complex forms and difficult to eliminate. Today, these substances are widely used in many industries, but their uncontrolled release has long-term adverse impacts on human health and the environment [2]. Indeed, when they accumulate in nature, these compounds can be absorbed by living organisms, disrupting their biological functioning. Some of them are toxic, carcinogenic, or can cause mutagenic and teratogenic effects, thus affecting the well-being of humans, plants, and animals [3]. Many industries, notably textiles, paper, food, cosmetics, and pharmaceuticals, discharge effluents loaded with synthetic dyes [4]. The massive use of these substances causes major water pollution, characterized by a high load of suspended solids and persistent coloration, leading to harmful ecological effects on ecosystems and infectious diseases in humans and animals. For instance, quinoline yellow is a

quinophthalone dye made up of a combination of sodium salts that are disulfonates (80%), monosulfonates (15%), and trisulfonates (7%) [5]. It is vastly exploited in the food, cosmetic, and pharmaceutical industries [6], presents a number of concerns, and is regarded as one of the hazardous environmental colorants [7]. Although Quinoline Yellow (E104) improves the coloring of products, its use is strictly monitored by health authorities. The European Food Safety Authority (EFSA) has set the Acceptable Daily Intake (ADI) at 0.5 mg per kg of body weight per day, which represents the maximum amount that can be consumed each day without risk to health. However, this substance can be harmful to sensitive individuals, even at doses below this threshold [8]. It is prohibited in foods intended for infants and young children and causes allergic reactions and digestive disorders due to their toxicity, non-biodegradability and carcinogenic potential [9].

In reality, the removal of dyes from wastewater is a challenge for the industries involved, as the synthetic dyes used are stable compounds that are difficult to destroy with conventional treatments. Physical, chemical, and biological methods are currently available for the treatment of wastewater discharged by various industries. However, physical methods such as liquid-liquid extraction, ion exchange, coagulation, flocculation, ozonation, ultrafiltration, reverse osmosis, adsorption, and air or steam stripping [10] are sometimes ineffective against certain highly resistant cases, and they have other disadvantages since they simply transfer pollutants to another phase [11]. In the face of this observation, the advanced oxidation process (AOP), particularly the Fenton process, stands out as the most effective. POAs use super powerful oxidizing agents such as hydroxyl radicals (·OH) and sulfate radicals to rapidly and efficiently degrade organic pollutants, including dyes. These processes are known to be highly effective, environmentally friendly, and capable of breaking down even the most resistant organic compounds into harmless products like carbon dioxide and water [12]. This technique not only completely eliminates pollutants, but also reduces the overall toxicity of effluents [13]. Their effectiveness is mainly based on the generation of very powerful reactive species such as hydroxyl radicals, which directly attack toxic compounds and transform them into harmless substances, easily removed

from the water [14]. This method is simple, effective and inexpensive, with great potential for application in wastewater treatment. In order to reduce costs, particularly related to reagents, it would be relevant to favor the use of abundant local resources such as clays [15,16], zeolites [17,18] and activated carbon debris from biomass residues [19]. These approaches are often combined with advanced oxidation processes (AOPs) to improve overall performance [20]. Thanks to their local availability, activated carbon debris can be integrated into the production of catalytic materials for advanced oxidation processes. Thus, their use in processes such as Fenton would improve the degradation of pollutants such as quinoline yellow dye, while reducing dependence on imported materials [3].

However, current advances aim to make this process heterogeneous, by immobilizing iron oxides or more broadly, transition materials on various support materials, such as activated carbon or Cu-Al/Biochar@g-C_3N_4 composites. In other words, we seek to fix these catalysts on solid supports in order to facilitate their recovery and reuse while improving their stability and efficiency in the treatment of polluted water. In Cameroon, across the entire national territory, coal and wood represent respectively 30.6% and 82.3% of household energy consumption, according to the United Nations Development Program [21]. In certain regions of the country such as the Far North and in rural areas, there is approximately 95% of the greatest use of wood fire as cooking energy. This increased use of wood and coal, which involves deforestation, is one of the causes responsible for greenhouse gas emissions and pollution. It also poses a threat to the preservation of food security and biodiversity. To address this, we will synthesize Cu-Al/Biochar@g-C_3N_4 from biochar to rid our wastewater of contaminants.

Biochars, obtained from plant biomasses, are carbon-based materials that offer advantages for the removal of pollutants in aqueous solution [22]. Indeed, they are inexpensive and have large specific surface areas, making them suitable for pollutant adsorption [23]. However, biochars have some limitations, including fine particles and reduced density, which make it difficult to separate pollutants from water. In addition, minimal surface functionalization result in a low capacity for adsorption [24]. To resolve such

limitations and raise adsorption capacity of toxic elements, It is suggested that biochars be modified to optimize their physicochemical properties, as suggested by the studies of Chemerys and Baltrėnaitė in 2018 [25]. In this perspective, heteroatom doping has received particular attention recently [26]. Alongside heteroatomic doping, the incorporation of metals into biochar's amorphous matrix offers a promising strategy to enhance its characteristics [27]. As an illustration, In 2016, Lian and colleagues produced a biochar enriched with nitrogen using corn straw. Nitrogen doping resulted in a considerable optimization of the biochar's structural attributes. The results of adsorption tests also showed that the doped biochar exhibited a significantly higher adsorption capacity than the undoped biochar, demonstrating adsorption capacities of 292 mg/g for Acid Orange 7 and 436 mg/g for Methylene Blue. More recently Tchuifon et al., 2025 investigated the effective retrieve of tetracycline and norfloxacin contaminants in wastewater using Cu-Al/Biochar@g-C_3N_4 as a low-cost sorbent [28]. The results of this study showed that the maximum adsorbed amounts were 65 and 96 mg/g, respectively, at specific pHs and with an optimal amount of adsorbent. These results revealed up to 90 and 82% removal percentages, which were impressive.

Several methods have been proposed to remove quinoline yellow from wastewater, including simultaneous removal assisted by ultrasound using a MOF-5 (metal-organic framework) hybrid, activated carbon (AC-MOF-5), and HKUST-1-MOF hybrid activated carbon [29,30], the use of zinc oxide nanoparticles loaded onto Na- and K-doped activated carbon for simultaneous removal using ultrasound and a central composite design (CCD) [31], heterogeneous Fenton and photo-Fenton processes in the presence of CuO/Fe_2O_3 [5] and heterogeneous Fenton in the presence of Zeolite-4A/Fe_3O_4 [7]. However, the majority of these studies have not addressed the doping of a Cu-Al/Biochar@g-C_3N_4 catalytic support from activated carbon for the removal of quinoline yellow. Although the use of biochars and graphitic carbon nitride (g- C_3N_4) is documented in the literature, the present study stands out by the design of a multi-component composite Cu-Al/Biochar@g- C_3N_4, whose synergistic doping by a bimetallic system (Cu-Al) combined with graphitic carbon nitride optimizes electron transfer during the heterogeneous Fenton process. This study demonstrates remarkable efficiency on high concentrations of quinoline yellow, thus meeting the real constraints of industrial effluents. This performance is supported by rigorous

optimization through the Response Surface Methodology (RSM) and a Box-Behnken Design (BBD), allowing to accurately model the interactions between pH, mass, H_2O_2 concentration, and pollutant load for a future intensification of the process on a larger scale. In short, the BBD method is a good statistical tool for designing and optimizing the process under study [32]. To better predict the overall effects of each variable on the process and how they interact with each other, the response surface methodology (RSM) is actually a set of mathematical and statistical techniques used to design experiments, create models, and determine the ideal conditions for the effect of independent variables on a dependent variable [33].

In view of the above, the main objective of this research is to study the degradation and optimization phenomena of the quinoline yellow pollutant using the Box-Behnken experimental design (BBD) with the response surface method (RSM), employing a catalyst synthesized from coal debris waste@Cu- and Al-doped g-C_3N_4 to determine, through the heterogeneous Fenton process, the optimal parameters of degradation including pH, pollutant concentration, and hydrogen (H_2O_2)

2. Experiment

2.1. Materials and chemicals

E104 (Quinoline yellow dye) has been purchased for the food industry on behalf of the First Africa Company, based in Douala, Cameroon. $CuSO_4.5H_2O$ (99%) and $Al(OH)_3.xH_2O$ (99%) were supplied by GHTECH (Guangdong Guanghua SciTech Co. Ltd., China). KCl (99.5%), HNO_3, and NaOH (98%) were supplied by Sigma Aldrich in Germany, whereas $CO(NH_2)_2$ (98%) was supplied by Fischer Scientific International Company in the USA. The chemical industry Prolabo has been used to manufacture 50% H_2O_2 and 99.5% methanol. Biochar was bought from charcoal vendors in PK14 market (Douala 5 sub-division).

2.2. Preparation of raw material and synthesis of catalyst

The biochar debris was first gathered and sorted. To get a suitable particle size, 300g was sorted, crushed, and sieved through a 150 µm sieve. To exclude water, the powder was sieved and then dried for 24 hours at 105°C. Coating was used to create Cu-Al/Biochar@g-C_3N_4 in a single step. This was accomplished by adding 20-g portion of biochar, 5-g portion of $CuSO_4.5H_2O$, 5-g portion of $Al(OH)_3$ x H_2O, and 10-g portion of $CO(NH_2)_2$ to a porcelain mortar and thoroughly mixing them. After that, the mixture was heated at 105

°C for a full day. After the mixture was dried, calcined for 24 hours at 550 °C, and cleaned in a 50% H_2O/ethanol mixture, the result was Cu-Al/Biochar@g-C_3N_4. The schematic of preparation process of Cu-Al/Biochar@g-C_3N_4 is shown in **Fig. 1**

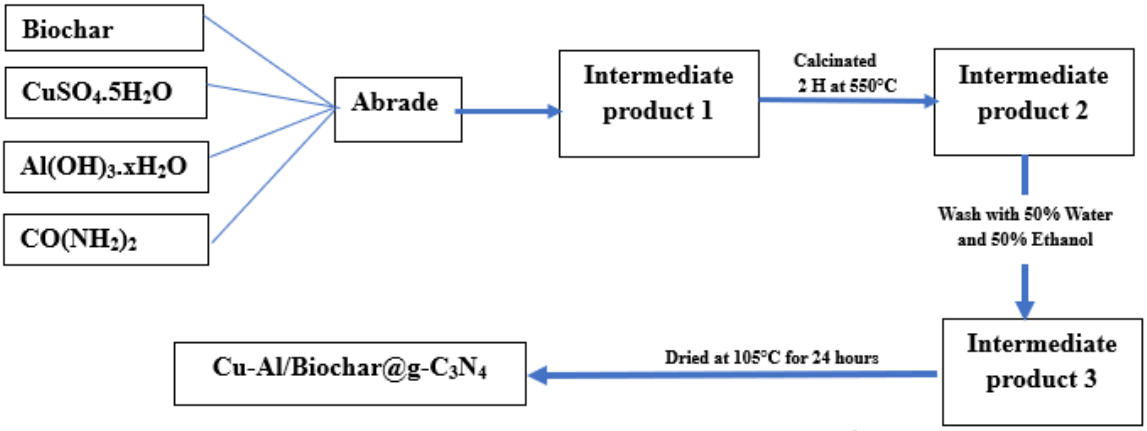

Fig. 1. The schematic of one-step synthesis of Cu-Al/Biochar@g-C_3N_4 nanosheet catalyst

2.4. Characterization techniques

The produced Cu-Al/Biochar@g-C_3N_4's physicochemical characteristics were investigated. The physicochemical characterization of the materials was conducted utilizing a suite of complementary analytical techniques. Fourier-transform infrared (FT-IR) spectroscopy was performed on a Nicolet Thermoscientific IS5 spectrophotometer to elucidate functional groups. Morphological and elemental composition was examined via scanning electron microscopy coupled with energy-dispersive X-ray spectroscopy (SEM/EDX) using a TESCAN VEGA 3-LMU instrument operated at an accelerating voltage of 8 kV. Crystalline structure and phase identification were ascertained by X-ray diffraction (XRD) analysis on a PANalytical X'Pert Pro diffractometer. The XRD measurements employed Cu-Kα1 radiation (λ = 1.54056 Å) at 40 kV and 30 mA, with a continuous scan from 10° to 90° (2θ) at a rate of 5° per minute.

2.5. Fenton oxidation tests

Catalytic activity of Cu-Al/Biochar@g-C_3N_4 was evaluated using Fenton oxidation studies. Cu-Al/Biochar@g-C_3N_4 (100, 150, and 200 mg) was combined with 120 mL of 100 mg/L E104 solution in a conical flask. Following

the addition of H_2O_2 (13, 39, and 65 mmol/L) to the mixture, the pH was adjusted between 2, 4, and 6 using solutions of NaOH and HNO_3 (10^{-3} mol/L). The suspension was stirred at room temperature at 150 rpm for 150 minutes. The residual E104 concentration in 8 mL samples taken at regular intervals was measured using UV-Vis spectrophotometry at 450 nm. The decomposition efficacy of E104 was computed exploiting Eq. 1: $R = \frac{C_o - C_t}{C_o} \times 100$ (1)

The terms C_0 (mg/L) and C_e (mg/L) denote the dye concentration at the beginning of the experiment and at adsorption equilibrium, respectively.

2.6. Optimization by RSM (response surface methodology)

The experimental design was constructed employing a Box-Behnken (BBD) design within the framework of response surface methodology (RSM), facilitated by Statgraphics Plus software (version 18.0). This investigation encompassed the optimization of three governing parameters: the pH of the dye solution (x_1), the initial concentration of E104 dye (x_2), and the hydrogen peroxide (H_2O_2) concentration (x_3). The catalyst mass was held constant at 50 mg for all experimental runs. The three independent elements mentioned above are used to create a matrix with six center points (Equation 2) and 20 experimental trials to be carried out, coded as shown in Table 1. Each trial's reaction is represented by the fraction of degradation (Y).

$$N_r = 2^v + 2v + c = 2^3 + 2(3) + 6 = 20 \quad (2)$$

Here, *v* signifies the number of independent variables, *c* is the center point replicates, and Nr indicates the total runs required.

Table 1. Coding of experimental factors for 20 decomposition tests.

Variables	**Units**	**Codes**	**Level**		
			-1	**0**	**+1**
pH		x_1	2.0	4.0	6.0
[E104]	mg /L	x_2	50.0	75.0	100.0
[H_2O_2]	mmol /L	x_3	13	39	65

The 20 experiments were conducted in a single block in a randomized fashion to underestimate imacts of uncontrolled factors and situations.

A predictive mathematical model was formulated based on a second-order polynomial equation. This empirical model incorporates the interactions among experimental variables to assess their collective impact on the target response. Subsequently, the model's validity was evaluated by analyzing the correlation between its predictions and the empirical results.

$$Y = \beta_0 + \sum_{1}^{n} \beta_1 x_1 + \sum_{1}^{n} \beta_{11} x_1^2 + \sum_{1}^{n} \sum_{1}^{n} \beta_{12} x_1 x_2 + \varepsilon \quad (3)$$

The model output Y is defined by a quadratic function featuring an intercept β_0, linear (β_1) and second-order (β_{11}) terms, a two-factor interaction (β_{12}), and the coded parameters x_1 and x_2.

2.7. Kinetic considerations of dye decomposition

Using preset ideal circumstances for each variable, the degradation experiment was kinetically modeled. For the degradation reactions, first-order and second-order linear kinetic rate laws were utilized by Eqs. (4) and (5), respectively.

First order: $\ln \frac{C_o}{C_t} = k_1 t$ (4)

Second order: $\frac{1}{C_t} - \frac{1}{C_o} = k_2 t$ (5)

2.8. Reusability studies

During three degradation experiments, the Cu-Al/Biochar@g-C_3N_4 composite's capacity to sustain its catalytic efficiency was assessed. 150 mg of Cu-Al/Biochar@g-C_3N_4 in 120 mL of dye solution at the ideal concentration and pH of the experimental design were used in the first test. The mixture (in a conical flask) was then supplemented with H_2O_2 at a predefined ideal concentration. After a maximum of 150 minutes of stirring, 8 milliliters were filtered and subjected to UV-visible spectrophotometric analysis. Equation 1 was used to determine the percentage of dye degradation in this initial test. Following this initial test, the Cu-Al/Biochar@g-C_3N_4 composite was extracted from the solution by magnetic separation. Centrifugation was used three times at 4000 rpm for eight minutes to wash the recovered material with deionized water. The material was employed in the subsequent deterioration experiment after being cleaned and oven-dried for four hours at 100°C. To get findings for

three consecutive cycles of experimental tests, two further tests were conducted, and the associated percentages of dye degradation were computed [34].

3. RESULTS AND DISCUSSION

3.1 X-ray diffraction (XRD) and Fourier transform infrared (FTIR)

X-ray diffraction is the main technique for characterizing crystalline phases, to determine their nature, structure and possibly to analyze the degree of crystallinity. A decrease in crystallinity is reflected on the diagram by a decrease in the intensity of the lines or a slight broadening of the lines.

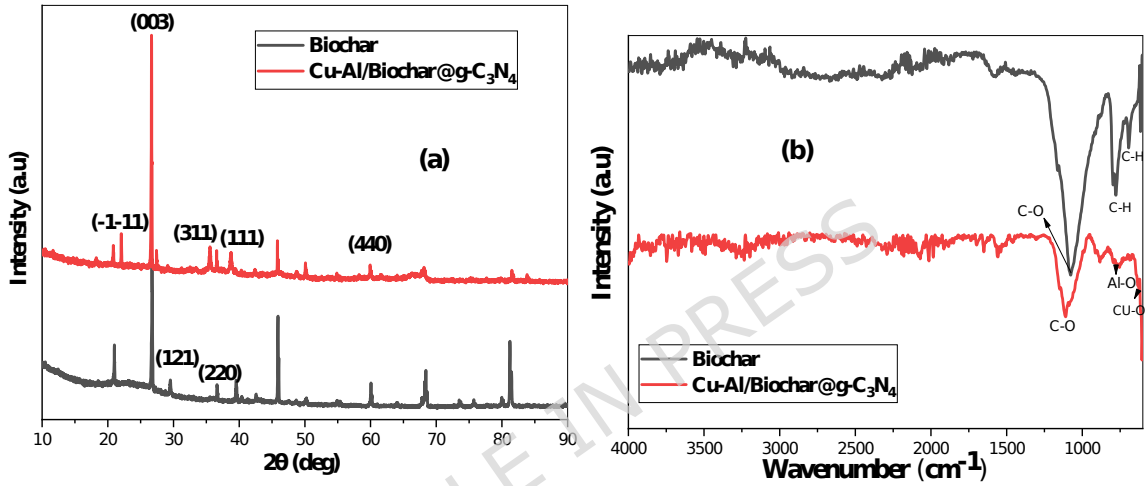

Fig. 2. XRD (a) and FT-IR (b) spectra of Biochar and Cu-Al/Biochar@g-C_3N_4

X-ray diffraction (XRD) analysis was performed to determine the crystal structure and mineral phases present in the raw biochar as well as in the modified Cu-Al/Biochar@g-C_3N_4. The corresponding diffractogram is presented in (**Fig. 2a)**. The XRD pattern of the biochar vouchsafes absence of crystalline peaks compared to that of the doped sample. This means that the biochar prepared from coal debris is predominantly amorphous [3]. However, it presents broad and low intensity diffraction peaks, notably around 2θ = 20.8°, 26.6°, 33.2° and 29.6°, corresponding respectively to the different planar crystalline structure of carbon [14], to the presence of calcite ($CaCO_3$) [35] and magnesite ($MgCO_3$) in the characteristic biochar of the amorphous or partially graphitized structure of carbon, typically of biochars pyrolyzed at moderate temperature [36]. After doping with copper, aluminum and nitrogen the material retains these characteristic peaks of biochar, and a clear

modification of the XRD profile is observed with the appearance of several new intense crystalline peaks. In particular, an intense peak at 36.5° and 59.9° attributed to the (311) and (440) plane of spinel $CuAl_2O_4$, which is consistent with the reference standards (PDF 01 -0704035) and that of Weizhong et al., 2009 [37]. The presence of peaks at 35.5° (plane 111) and 38.7° (plane 200) could also indicate the formation of copper oxides such as CuO [38] (Allwar A, Ahdiaty R, 2022) or Cu_2O [39]. The copper (I) oxide's planes of (200) and (222), respectively, and the development of an Al/Cu bi-metallic structure on biochar's surface are therefore responsible for the peaks that occur at 2θ = 42.5 and 79.8° and improvement of peaks at 39.50 and 45.85° (2θ) [28]. Furthermore, successful assimilation of the metallic elements (Cu, Al) and structural alteration of material are confirmed by the formation of these new crystalline phases and the partial elimination of the distinctive peaks of the raw biochar.

The Debye-Scherrer equation was used to determine the crystallite size of the biochar and Cu-Al/Biochar@g-C_3N_4 from XRD data, given by [40,41]:

$$D = \frac{K\lambda}{\beta \cos\theta}$$

Provides a method to calculate the average crystallite size. In this equation, D represents the average crystallite size in nanometers (nm), K is the Scherrer constant, λ is the X-ray wavelength (for CuKα, λ=1.5406 A◦), β is the line broadening at full width at half maximum (FWHM) in radians, and θ is the Bragg angle, which is half of 2θ. Using the Debye-Scherrer equation, the average size of the crystallite grains was calculated to be 7.726 and 16.677 nm, respectively for the biochar and Cu-Al/Biochar@g-C_3N_4.

The significant average crystallite size difference between the crystallites of pure biochar (7.726 nm) and Cu-Al/Biochar@ g-C_3N_4 (16.677 nm) indicates that the modification considerably influences the crystal structure. This variation could also signal more efficient crystal lattice structuring in the Cu-Al/Biochar@g-C_3N_4 composite, which could offer benefits for several applications, including pollutant adsorption, heterogeneous catalysis, and electronic conductivity [42]. Observations indicate that the alteration of biochar with copper, aluminum, and γ-C_3N_4

significantly increased the crystallite size, from 7.726 nm to 16.677 nm. This suggests an improvement in the material's crystallinity, which could influence its physical and chemical properties, particularly in the areas of adsorption and catalysis. The increase in crystallite size is likely attributable to the agglomeration and organization of crystals by modifying elements such as copper, aluminum, and g-C_3N_4.

The infrared spectrum of the samples (**Fig. 2b)** shows that the band around 1000–1100 cm^{-1} (CO) indicates the presence of C=O typical bonds of the carboxylic phenolic groups or alcoholics. A more marked intensity in the doped biochar suggests increased surface activation, favorable to the degradation of pollutants [43,44]. The band around 600–750 cm^{-1} (Al–O) is the characteristic signal of the aluminum-oxygen bond, indicating that aluminum has been successfully integrated into the biochar matrix. This confirms the formation of oxides aluminum or aluminates [45,46]. The successful incorporation of these minerals into the biochar matrix is spectroscopically confirmed by the emergence of distinct absorption bands within the 500–800 cm^{-1} region, specifically corresponding to Cu–O vibrations at 625.0 cm^{-1} and Al–O vibrations at roughly 781.3 cm^{-1} [28]. These observations confirm the enrichment of the biochar surface in various functional groups.

3.2. SEM -EDX analysis

SEM observation (**Fig. 3a)** of raw biochar shows a relatively smooth surface, with parallel striations and vertical sheet-like or channel-like structures. The texture appears to be low in porosity and roughness. This is typically of biochars obtained by pyrolysis at moderate temperatures (between 400–600°C). The structure is generally more compact with less porosity development [47]. SEM (**Fig. 3b)** of modified biochar (Cu-Al/Biochar@g-C_3N_4) shows that the surface is much rougher with a granular appearance, clearly visible spherical or irregular aggregates. A significant increase in porosity and particles attached to the surface is observed. This clearly indicates a modification of the structure following doping. The incorporation of metals (Al and Cu) and nitrogen (N) generally leads to an increase in active sites and an improvement in the specific surface area and pore texture. This is consistent

with previous work showing that metal doping induces the creation of new porous structures and surface roughness [48].

For the EDX results of the biochars (raw and Cu-Al/Biochar@g-C_3N_4), the raw biochar (**Fig. 3c)** shows the majority presence of the elements Carbon (C) and Oxygen (O), representing respectively approximately 33.9% and 60.4% in atomic weight. This composition is typically a biochar resulting from pyrolysis, rich in carbon with a high oxygen content due to the oxygenated functional groups (hydroxyls, carbonyls, carboxyls, etc.) still present on surface of the biochar [47]. After modifying (**Fig. 3d)**, we observe the presence of new elements such as Al (27.2%), Cu (41.7%), N (1.7%), Si (4.3%) and S (5.3%). Oxygen is still present (21.7%) but in a lower proportion than in the raw biochar, due to the partial replacement by metals. The high content of Cu and Al confirms that the doping process allowed an effective impregnation of metals on the surface of the biochar. The presence of nitrogen (N) is not directly visible here because the EDX technique poorly detects light elements such as nitrogen, this can also be justified by the traces remaining after washing the modified composite. However, the relative decrease in the C/O ratio and the increase in metals indirectly support the success of the doping [49].

(**Fig. 3e)** shows a clear dominance of carbon (79%) and oxygen (8%), classic constituent elements of biochar. We also note the presence of low percentages of magnesium, calcium and iron, from organic raw materials or the pyrolysis process.

The homogeneity of the elements indicates a relatively clean surface, without external metallic impregnation. (**Fig. 3f)** reveals the distinct and localized presence of copper (Cu), aluminum (Al) and nitrogen (N), confirming the successful functionalization of the biochar. Carbon (32%) remains the majority, but the metals are well dispersed, indicating good incorporation into the carbon matrix. Nitrogen, coming from doping, is well distributed, which favors the improvement of the active sites for catalysis and adsorption. The presence of elements such as sulfur (S) and silicon (Si) could be related to the precursors or the synthesis environment.

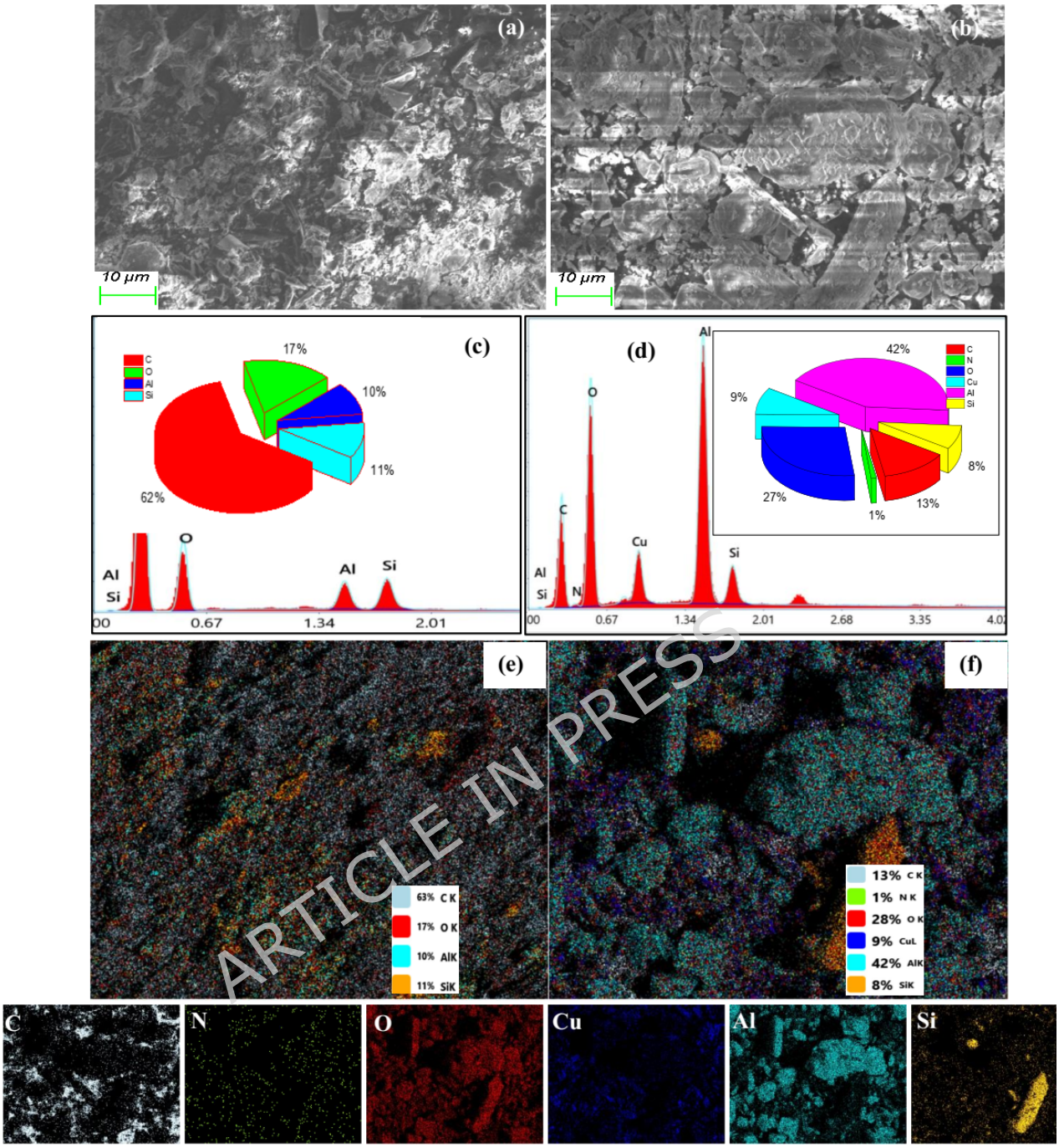

Fig. 3. SEM, EDX and mapping analysis of Biochar (a, c, e) and Cu-Al/Biochar@g-C_3N_4 (b, d,f)

The evolution of the final pH as a function of the initial pH is depicted by the curve in Figure—4. The pHpzc is found at the intersection of the experimental curve and the line of $pH_f = pH_i$. This material's $pH_{pzc} = 6.2$ (visual estimate) indicates that the surface is positively charged at pH < 6.2, which is advantageous for the adsorption of anions, and negatively charged at pH > 6.2, which is advantageous for the adsorption of metal cations.

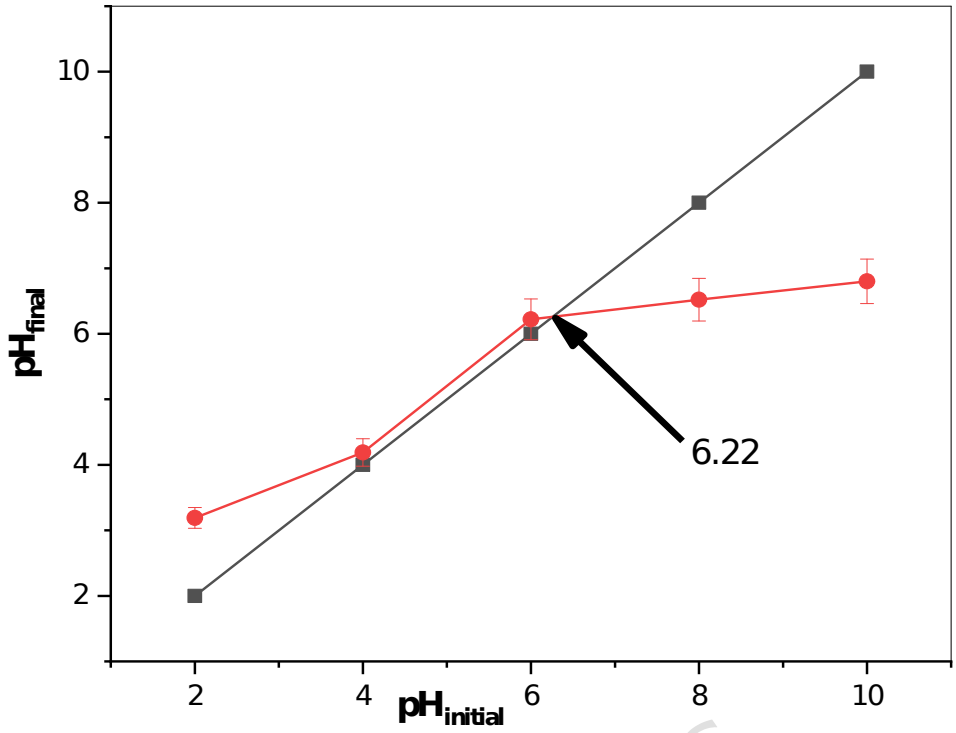

Fig. 4. pH_{pzc} of Cu-Al/Biochar@g-C_3N_4

3.4. Degradation of Quinoline Yellow in Aqueous Solution by the Fenton Process

3.4.1 Influence of parameters influencing the Fenton process

- **Influence of pH**

The study **(Fig. 5a)** shows that the effect of pH on the efficiency of the Fenton process is significant. Three pH values were tested (2, 4 and 6). The results reveal that quinoline yellow's decomposition is maximum at pH 2. At this pH, the efficiency reaches 70% which is higher than that obtained at pH 4 and 6. However, due to iron sludge development and iron leakage from the biochar structure, their activity dramatically drops at values of 4 and 6. At neutral pH, the iron ions then precipitate as iron sludge $Fe(OH)_3$. It is also observed that because hydrogen peroxide (H_2O_2) self-destructs, this pH rise reduces the hydroxyl radical's oxidation potential. In this case, the Fenton-type catalytic cycle is encouraged by the biochar-doped Cu/Al in the reaction solution, which guarantees ongoing regeneration of Fe^{2+} ions [28]. Therefore, the dye degrades more when the pH is lower. This outcome stems from the dissolution of substantial iron from the catalyst at pH 2, releasing ferrous and ferric ions

into solution. These ions subsequently react with residual hydrogen peroxide, thereby inducing homogeneous Fenton process. This homogeneous catalysis then complements the heterogeneous catalysis, which improves the overall efficiency of the degradation process. In other words, this phenomenon results from the decomposition of H_2O_2 into O_2 and H_2O accompanied by the formation of iron hydroxide, which actively participates in the degradation reaction. A limitation of the Fenton process, however, is the restricted pH range in which it is effective [7]. However, the decrease at pH 6 is due to the presence of iron hydroxide and the production of a ferric hydroxide precipitate. These observations confirm that the Fenton process works best in acidic media, with an optimal pH between 2 and 4 as confirmed by other studies. Thus, maintaining an acidic pH which is essential to optimize the efficiency of dye treatment by the Fenton process. The increase in pH 6 relative to pH 4 between 100 and 150 minutes can be elucidated by the reality that, within this range, the percentage of degradation augments to a saturation point. Beyond this point, a further increase in H_2O_2 leads to a decrease in elimination efficiency [50], as observed during the first 80 minutes.

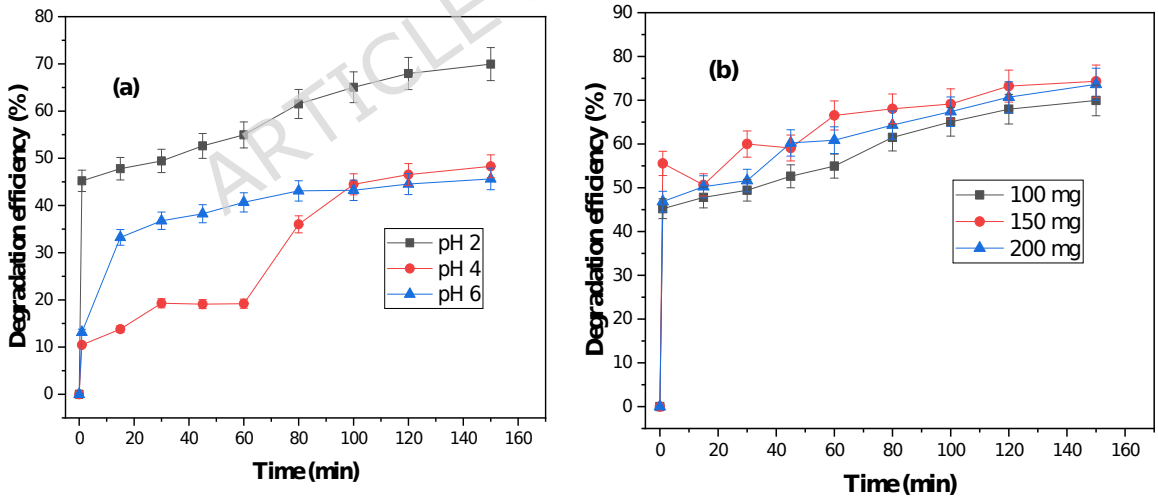

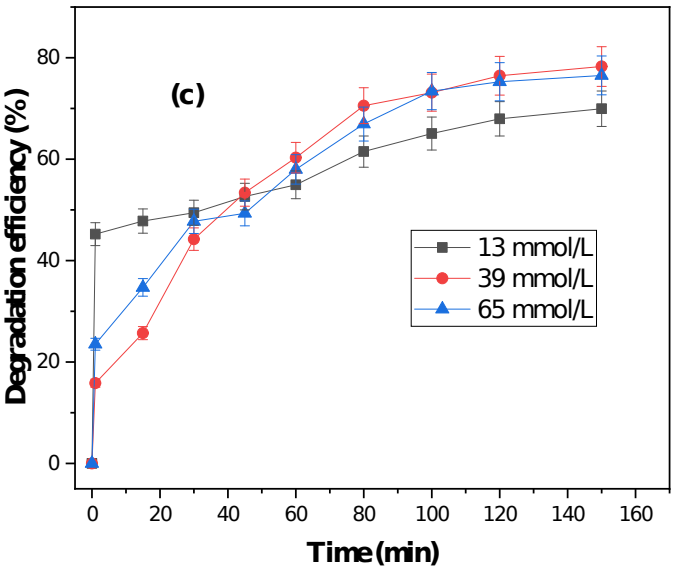

Fig. 5. Influence of pH (a), mass (b), and H_2O_2 concentration (c) on the degradation of E104

quinoline yellow degradation

- **The influences of catalyst mass**

Fig**. 5b** illustrates the influence of catalyst mass as a function of time. It is observed that when the concentration of the pollutant or dye is hold constant, and the contact time remains unchanged, increasing the mass of the material or catalyst from 100 to 200 mg improves the degradation efficiency. This improvement comes from having more active sites available at higher adsorbent concentrations, making it easier to remove a larger amount of the pollutant. As the adsorbent dose goes up, more sites are exposed, providing more opportunities for bonding with quinoline yellow molecules. The increase in surface area and number of active sites makes it easier for the adsorbent to capture more quinoline yellow molecule [51]. After 150 minutes, the degradation rate increases from 69.95 to 74.31% with 100 and 150 mg of catalyst respectively. This improvement is explained by the presence of more active sites on the material, which promotes the formation of hydroxyl radicals (OH $^{\bullet}$) [52]. However, beyond 150 mg, the efficiency stagnates due to the saturation of the catalytic sites or a limited amount of hydrogen peroxide reacting with the available iron. When the catalyst mass is higher, more hydrogen peroxide is consumed to regenerate radicals, but if the hydrogen peroxide is completely consumed, there is no longer an efficient Fenton reaction [7]. It is also noted that a total amount of hydrogen peroxide completely reigns with the available Fe^{2+} to form Fe^{3+}. This

indicates that a good balance between the amount of hydrogen peroxide and the catalyst is required to maintain a continuous production of radicals essential for the decomposition of pollutant. When catalyst mass is increased to 150 and 200 mg, a desorption phenomenon of the pollutant is observed at 20, 35, and 45 minutes, respectively. This can be explained by the fact that, at some point, adsorption reached equilibrium, and then the added H_2O_2 initiated the catalytic oxidation process, resulting in a 74% acceleration of the degradation rate within the following 105 minutes.

- **Influence of the concentration of hydrogen peroxide H_2O_2**

Fig. 5c shows that increasing the concentration of hydrogen peroxide from 13 to 65 mmol/L leads to an increase in the percentage of degradation of the pollutant from 69.95% to 78.27% at 150 min for the respective concentrations 13 and 39 mmol/L. The percentage of degradation depends on the concentration of hydrogen peroxide. Many researches have suggested that the addition of oxidizing agents such as hydrogen peroxide can limit the effects of recombination by reacting [7] quickly with the electrons present in the conduction band. This interaction promotes the formation of highly reactive oxidizing species [53]. However, increasing the peroxide dose increases the reaction rate and thus improves the pollutant degradation efficiency up to the saturation point. Beyond this point, further increases slow down degradation. This is due to the scavenging effect of peroxide on hydroxyl radicals (HO•), as described by equations (6) and (7), which can explain the degradation kinetics of E104 at a concentration of 65 mmol/L [50].

$$H_2O_2 + HO\bullet \rightarrow HO_2\bullet + H_2O \quad (6)$$

$$HO_2\bullet + HO\bullet \rightarrow H_2O + O_2 \quad (7)$$

In a conventional manner, the formation of hydroxyl radicals and the decomposition of hydrogen peroxide can be represented by the following reactions [54].

$$H_2O_2 + e^- \rightarrow OH^- + OH^\bullet \quad (8)$$

$$2\ H_2O_2 + \text{Energy} \rightarrow 2\ OH^\bullet \quad (9)$$

$$H_2O_2 + H^+ + e^- \rightarrow OH^\bullet + H_2O \quad (10)$$

$$H_2O_2 + O_2^{\bullet -} \rightarrow OH^\bullet + OH^- + O_2 \quad (11)$$

According to the earlier equations, the availability of hydrogen peroxide increases the production of OH• hydroxyl radicals, which raises the rate of oxidation. The study's findings are consistent with those documented in the literature [3]. During the process, the transformation of the ferrous ion in the presence of hydrogen peroxide and hydroxyl radicals constitutes an advantage for the Fenton reaction. This mechanism promotes the formation of $OH^{\bullet}$ radicals in greater quantity, which allows for enhanced degradation of the organic compounds present.

3.4.2 Application of response surface method for quinoline yellow removal by fenton process using Cu-Al/Biochar@g-C_3N_4 catalyst

Within the framework of the RSM, a collection of mathematical and statistical techniques for designing experiments, creating models, and assessing the effects of factors, Design-Expert 13 software was used in this study to optimize experimental conditions for the catalyst's degradation of quinoline yellow using the centered composite design technique (Table 2).

Table 2. The centered composite design's experimental matrix for optimizing quinoline yellow degradation on the catalyst

No.	pH	Concentration of pollutants (mg/L)	Concentration in H_2O_2 (mmol/L)	Y: Degradation efficiency (%)	
				Observed value	Predicted value
1.	2	50	13	82.32	80.91
2.	6	50	13	48.12	53.11
3.	2	100	13	86.3	89.98
4.	6	100	13	81.34	78.60
5.	2	50	65	82.08	85.16
6.	6	50	65	86.38	83.04
7.	2	100	65	82.48	77.83
8.	6	100	65	90.37	92.12
9.	2	75	39	84.22	83.48
10.	6	75	39	77.4	76.72
11.	4	50	39	86.52	83.17
12.	4	100	39	90.31	92.25
13.	4	75	13	86.5	81.95
14.	4	75	65	87.7	90.84
15.	4	75	39	87.1	87.06
16.	4	75	39	86.47	87.06
17.	4	75	39	86.34	87.06
18.	4	75	39	86.47	87.06
19.	4	75	39	86.94	87.06
20.	4	75	39	86.24	87.06

Based on the experimental findings, an approximate regression model of bleaching efficiency was assessed and represented by the subsequent second-order polynomial equation :

The percentage of degradation = 75.5389 + 1.24536 x_1 - 0.0573595 x_2 + 2.94803x_3 - 1.73807 x_1^2 + 0.082075 $x_1 x_2$ + 1.60469 $x_1 x_3$ + 0.00104436 x_2^2 - 0.082025$x_2 x_3$ - 0.165568 x_3^2 (12)

In equation (12), x_1, x_2, x_3 are the corresponding coded variables of pH, pollutant concentration, and hydrogen peroxide concentration respectively. For every influence, the ANOVA table breaks down the variation in degrading efficiency into several components. Next, it compares the mean square to an estimate of the experimental error to determine each effect's statistical significance. Positive signs in front of the factors in the equation suggest a synergistic effect, whereas negative indications imply an antagonistic effect. The regression model in this instance produced a high coefficient of determination (R^2 = 90.56%). This suggests that the independent variables account for 90.56% of the variability in dye degradation efficiency, and that 9.44% of the variations cannot be explained by the model. The model's significant importance has also been demonstrated by the coefficient of determination adjusted ($R^2_{adjusted}$ = 82.07).

Table 3. ANOVA for the quadratic model

Source	Sum of Squares	df	Mean Square	F-value	P-value	
Model	1360.20	9	151.13	10.66	0.0005	Significant
x_1-pH	114.18	1	114.18	8.06	0.0176	
x_2-pollutant concentration	205.93	1	205.93	14.53	0.0034	
x_3-[H_2O_2]	197.40	1	197.40	13.93	0.0039	
$x_1 x_2$	134.73	1	134.73	9.51	0.0116	
$x_1 x_3$	329.60	1	329.60	23.26	0.0007	
$x_2 x_3$	134.56	1	134.56	9.49	0.0116	
x_1^2	132.92	1	132.92	9.38	0.0120	
x^2_2	1.17	1	1.17	0.0827	0.7796	
x^2_3	1.21	1	1.21	0.0851	0.7765	
Residual	141.73	10	14.17			
Lack of Fit	141.14	5	28.23	236.67	< 0.0001	Significant
Pure Error	0.5963	5	0.1193			
Total Horn	1501.94	19				

The model's F value of 10.66 (Table 3) suggests that it is significant. Such a high F value is just 0.05% likely to be the result of noise. P values larger than 0.05 show that the model's terms are not significant, but P values less than 0.05 show that they are. Important terms in this instance are x_1, x_2, x_3, x_1x_2, x_1x_3, x_2x_3, and x_1^2. The terms in the model are not important if the value is bigger than 0.1000. The concentration of the pollutant is the coefficient in the linear term and in the intermediate term and has a greater influence, as shown by the P values less than 0.05 for degradation of quinoline yellow, even though the majority of the parameters examined in this study have a significant impact on the degradation phenomenon. The fact that the concentration of the pollutant affects both the material's surface and the behavior of the pollutants in solution would support this observation.

A considerable misfit is implied by the misfit F-value of 236.67. This kind of misfit F-value has a 0.01% probability of being caused by noise. We want the model to be fit, so a large misfit is undesirable.

3.4.2.1. An overview of the modification

The correctness and fit of the model were assessed by statistical analysis utilizing the sequential model's sum of squares and model summary statistics. Table 4 displays the sequential model's sum of squares for E104 elimination. The quadratic model was recommended based on the results in Table 6 since the p value was less than 0.05 and the F value was 5.73. Additionally, as their difference (0.0847) is less than 0.2, the regression model results for E104 deterioration of Square (0.9056) and Adjusted Square (0.8207) were in reasonable agreement [55].

Table 4. Sum of Squares for a Sequential Model

Source	Sum of Squares	df	Mean Square	F-value	p - value	
Mean vs Total	1.397E+05	1	1.397E+05			
Linear vs. Mean	517.51	3	172.50	2.80	0.0733	
2FI vs Linear	598.89	3	199.63	6.73	0.0056	
Quadratic vs 2FI	243.80	3	81.27	5.73	0.0151	Suggested

Cubic vs Quadratic	136.63	4	34.16	40.14	0.0002	Aliased
Residual	5.11	6	0.8509			
Total	1.412E+05	20	7060.71			

3.4.2.2. Disturbance diagram

The perturbation plot illustrates the relative influence of each variable on the response at a specified point in the process. As depicted in **Fig. 6**, under conditions of pH 4, a pollutant concentration of 75 mg/L, and an H_2O_2 concentration of 39 mmol/L, the comparative effects are evident. In plot A, pH exhibits a shallower slope, indicating a more limited impact on the degradation percentage. Conversely, both pollutant concentration (C) and H_2O_2 concentration (D) demonstrate steeper slopes, reflecting a more pronounced positive influence on degradation efficiency. This observation is supported by the higher corresponding F-values (14.53 for C and 13.93 for D), as presented in **Table 3**.

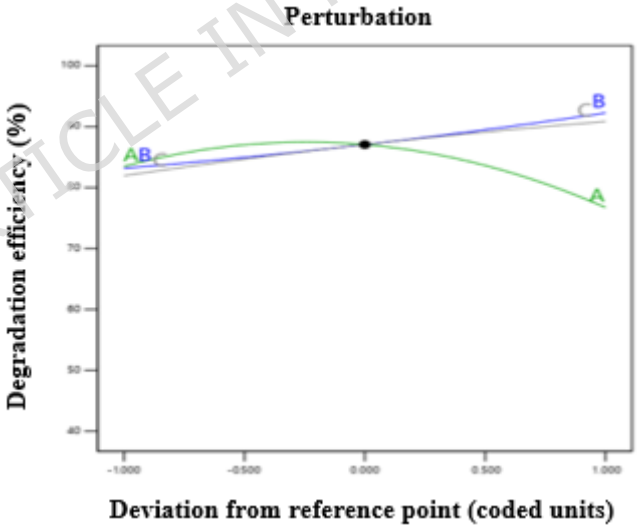

Fig. 6. Disturbance diagram

3.4.2.3. Response surface and design optimization

The response surface modeling is shown in three dimensions (3D) in the figure 6, which illustrates the independent and dependent effects of initial pH, catalyst mass, and H_2O_2 concentration on the elimination of quinoline yellow

via heterogeneous Fenton-type reactions on the catalyst. The relationship between initial pH and material mass, concentration, and H_2O_2 concentration, respectively, is shown in Fig. 7. Clearly, all three examples exhibit a similar pattern : the degradation efficiency rises as the initial pH rises, and 70% of the color is removed when the initial pH is at 2. because the material's surface has more active spots. Consequently, a rise in pH causes level of ions (H^+) in solution to drop, which encourages cations to adsorb on the anionic sorption sites of sorbents with strong electrostatic contacts. In fact, a high pH accelerates the breakdown of H_2O_2 into oxygen (O_2) and water (H_2O), which results in insufficient radical generation [32]. The improved composite's pH_{PZC} was determined to be 6.22 [56]. Nevertheless, the addition of H_2O_2 concentration accelerates the pollutant's breakdown because it increases the electrostatic attraction forces between the dye molecules absorbed on the catalyst's surface [57]. Nevertheless, an overabundance of H_2O_2 leads to the spontaneous self-decomposition of H_2O_2 into H_2O and O_2 molecules, as well as the breakdown of $^{\bullet}OH$ generated during the reaction into radicals with a lower oxidizing power ($HO_2^{\bullet}$ ions), which lowers the removal efficiency [58]. When the pollutant concentration increases from 50 to 100 mg/L, the efficiency decreases. This drop is related to the limited number of active sites compared to the larger amount of pollutant molecules in solution. On the other hand, at low concentrations, the active sites are sufficient to capture most of the quinoline yellow molecules, which results in better removal efficiency [59].

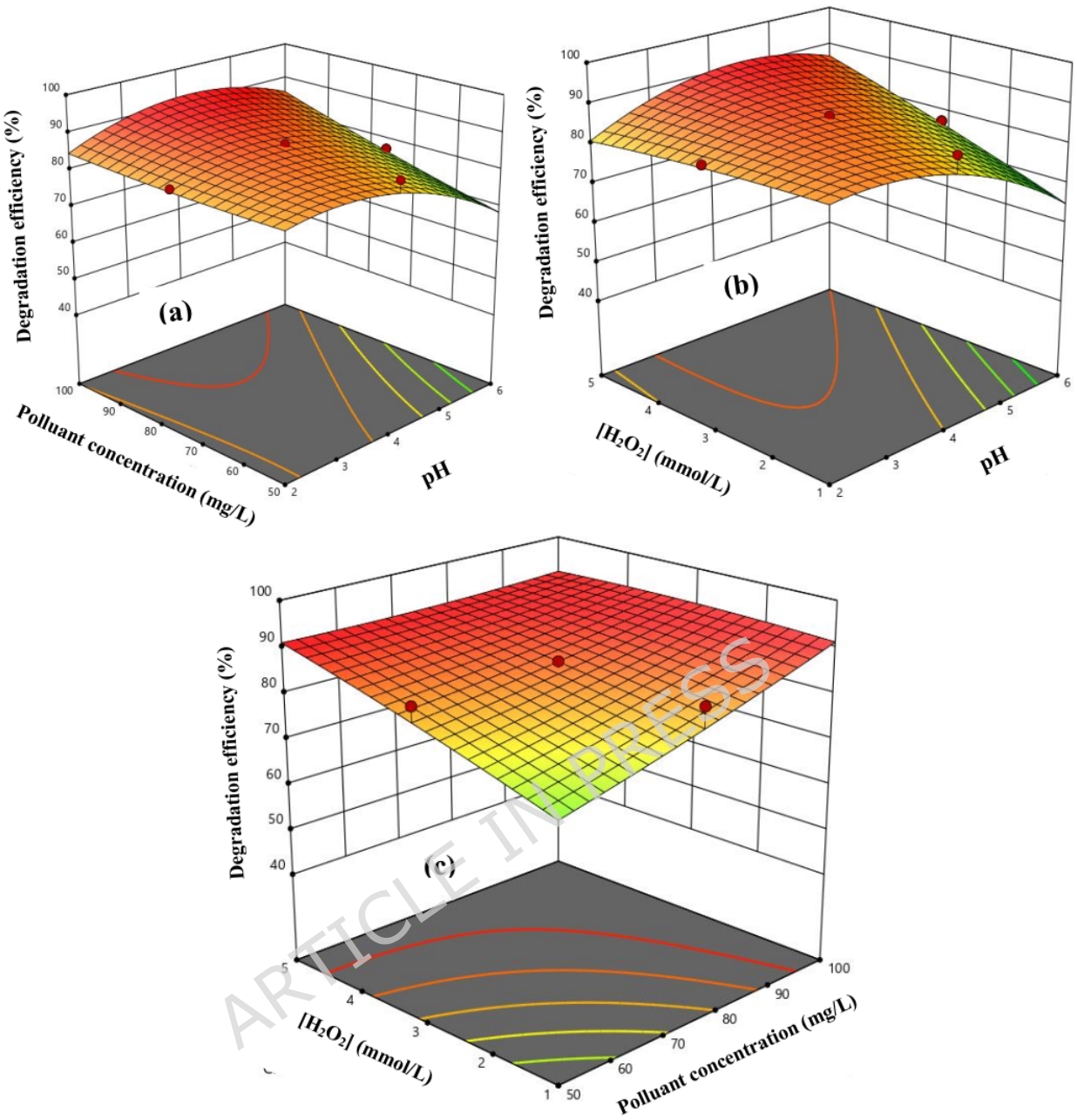

Fig 7. Assessment of key operational parameters, i.e., initial pollutant concentration, solution pH, and H_2O_2 dosage, on the decomposition efficacy of E104.

3.4.2.4. Validation and experimental confirmation of the model

Under ideal circumstances (pH = 5, catalysis mass = 50 mg, dye level = 100 mg/L, and H_2O_2 concentration = 65 mmol/L), the ideal process values variables for optimum degradation efficiency have been found. According to the suggested model, the deterioration efficiency under ideal circumstances was 93.60%. Confirmatory tests have been carried out and a decomposition rate of 92.33% was observed after 2h30 min of reaction time under optimal

conditions, which is well in line with the model predictions. This result is close to that of Foko et al., 2025 [7] on the degradation of E104 by the heterogeneous Fenton process at the same equilibrium time. This suggests that the method used in this study to optimize the decomposition circumstances and achieve the highest decomposition efficacy for the removal of quinoline yellow with the catalyst is effective.

3.5. Kinetic studies

Degradation kinetics is important to describe the degradation of E014 and time. To do this, two models were evaluated, namely the Pseudo first-order model and Pseudo second-order on the pH parameter. **Fig. 8a** presents the pH evolution graph in the Pseudo first-order model. It can be seen that the degradation kinetics is faster when the pH is low (pH=2) and that a variation in pH between 4 and 6 reduces the degradation rate, with a very low or negligible and almost horizontal at (pH=6). The same observation is made regarding the Pseudo second order model (**Fig. 8b)**, with the only difference that the correlation coefficients R^2 are a little higher at pH 2 and 4. These findings can be explained by the fact that increased interaction between the composite and the pollutant E104 makes it easier to produce oxidizing agents that encourage the compound's degradation and boost the process' catalytic efficiency. Additionally, because the composite's structure contains heteroatoms like nitrogen and oxygen, the surface functionalization functions as an electron giver and acceptor, influencing the process of radical production that will act in the pollutant's conversion and mineralization [60]. Consequently, it can be concluded that the Cu-Al/Biochar@g-C_3N_4 composite's degradation of the pollutant E104 is better described by the pseudo second order model.

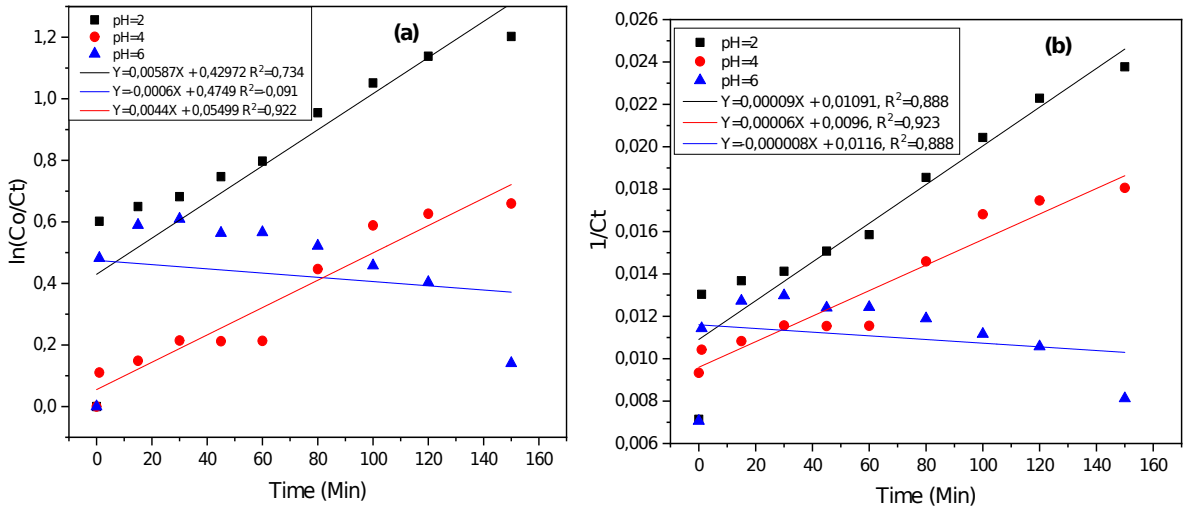

Fig.8. Pseudo-first (a) and pseudo-second-order (b) kinetic model of E104 degradation

3.6. Reuse of the catalyst

Finally, to evaluate the regeneration cycle, performance tests were carried out under optimal conditions (50 mg, pH: 5, [E104]: 100 mg/L, [H_2O_2]: 65 mM and 150 minutes) in a solution volume of 50 mL. The Fig. 9 looked at the prepared material's reuse efficiency. This was accomplished by centrifuging the catalyst out of the reaction mixture and repeating the procedure after three cycles of quinoline yellow degradation. After three consecutive cycles of degradation, the material's degradation efficiency dropped from 70.30 to 50.28%. This shows a significant reduction in degradation capacity due to pore blockage, changes in structure, and loss of active functional groups. Efficiency remains above 65% up to the second cycle, so the composite can be effectively reused twice before losing much of its effectiveness. Beyond that, its regeneration drops to 50%, which limits its long-term use [61]. The loss of material quantity and Cu-Al/Biochar@g-C_3N_4 leaching during dye degradation, as well as catalyst separation and washing following each cycle, could be the cause of the decline in degradation efficeiency (%). After three cycles of degradation trials, the catalytic activity has decreased by less than 18%. The degradation of some active sites by adsorbed E104 molecules may also be the cause of this decline. As a result, these materials show stability throughout three cycles of degradation [62].

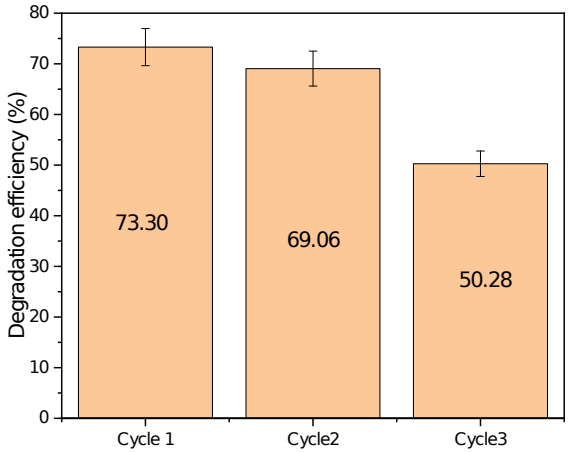

Fig. 9. Regeneration of Cu-Al/Biochar@g-C_3N_4 composite

Table 5 presents a comparison analysis between our research and published studies, highlighting the almost identical rate of degradation and demonstrating the material's effectiveness in the degradation of yellow quinoline in an aquatic environment.

Table 5. Comparison of the removal performance

Adsorbent	Degradation efficiency (%)	Optimal Conditions	references
ZnO–AC–NPs	90.16	10 mg/L, 0.02 g, pH 7, and 4 minutes of sonication	[26]
AC–HKUST-1- MOF	90.75	10 mg/L, 0.02 g, pH 4 and 4 minutes of sonication	[25]
AC–MOF-5	91.91	5.04 mg/L, 0.02 g, pH 7.59 and 2.55 minutes of sonication	[24]
Cu-Al/Biochar@g-C_3N_4	93.60	pH = 5, 50 mg, 100 mg/L, and [H_2O_2] 65 mmol/L and 150 minutes of reaction	This work

3.7. Graphical abstract proposal of the degradation mechanism

The **Fig.10** illustrates the diagram shows a summary of the heterogeneous Fenton degradation mechanism Cu-Al/Biochar@g-C_3N_4. During the reaction, the addition of hydrogen peroxide comes into contact with the metallic active sites on

the surface of the biochar. H_2O_2 is decomposed to produce hydroxyl radicals (•OH) [12]. These species, highly oxidative and non-selective, capable of breaking complex organic molecules, attack the structure of quinoline yellow and transform it into smaller and less toxic molecules (degradation by-products). Under the continuous action of the radicals, these intermediates are completely degraded to yield the inorganic products H_2O and CO_2 as well as NO_3^- ions.

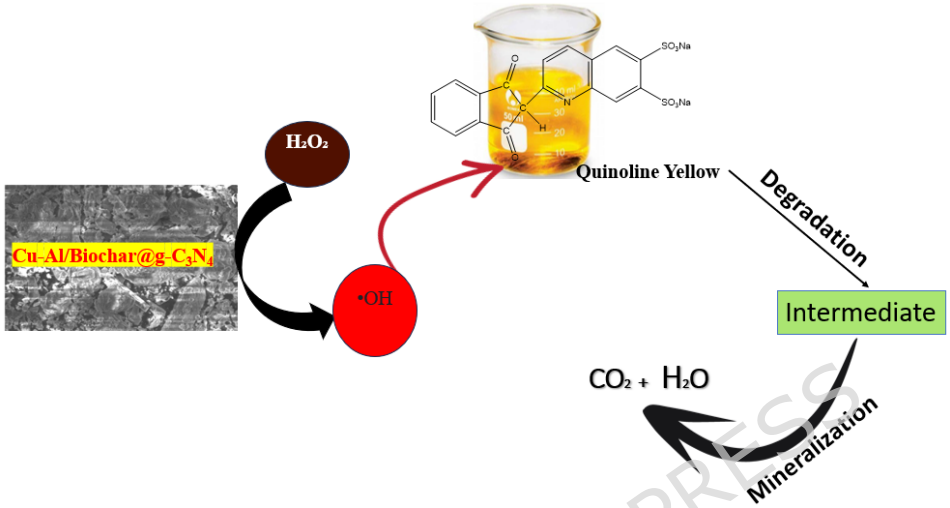

Fig. 10. Summary of Schematic Illustration of the Degradation Mechanism of Quinoline Yellow

3.8. Characterization of the composite after degradation

Fig. 11 presents the SEM, EDX, and XRD results of the material after pollutant degradation.

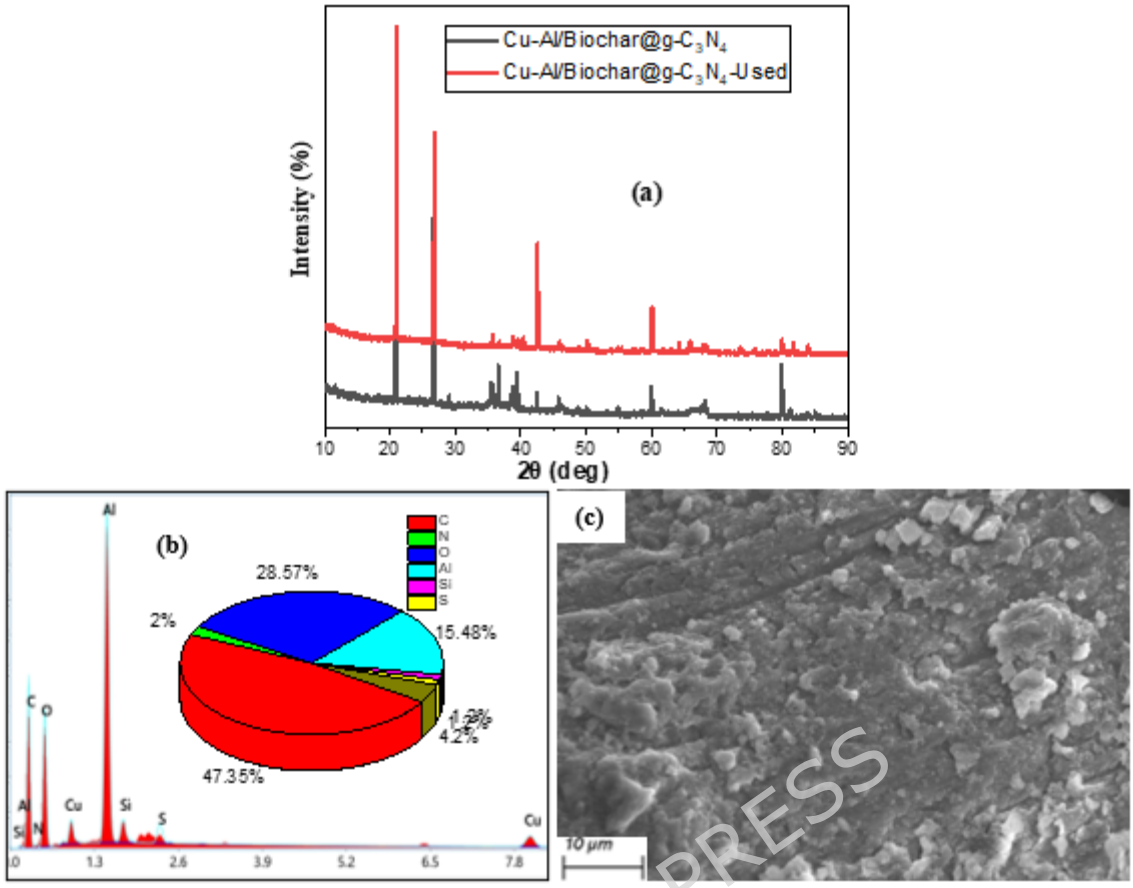

Fig. 11. XRD (a), EDX (b) and MEB (c) of Cu-Al/Biochar@g-C_3N_4 after degradation reaction

The fact that the degradation process of the composite had no effect on the crystalline structure of the charcoal (Fig. 11a) suggests that the X-ray diffraction peaks did not alter the initial structure of the material after degradation. However, it is observed that the peak shifts to 29.4°, indicating a slight increase in the interplanar spacing, suggesting a slight stretching of the distance between layers in the graphene structure. On the other hand, the crystalline plane around 43.9° shows small changes in the carbon peak due to the degradation of quinoline yellow, with variations in the layer spacing [61]. Thus, a change in the elemental composition is visible on the EDX spectrum (Fig. 11b). Elements (Mg, Fe, K, and Ca) are absent, while the percentages of the other elements aside from oxygen, which has stayed constan-vary. Leaching of the elements (Mg, Fe, K, and Ca) during the reaction or material washing can account for their absence. The mineralization of atoms from the pollutant's breakdown could be the cause of the rise in carbon and nitrogen content. Additionally, some copper (Cu) was liberated, which could account

for the composite's diminished efficacy after three reuse cycles. However, other peaks, particularly those at 2θ = 36.5° and 70°, may have decreased in intensity or disappeared, supporting the theory that the metals absorbed into the biochar were leached away. The material's structure has slightly changed, though, as seen in Fig. 11c, where it is less rough and has clearly visible spherical or irregular aggregates.

Conclusion

This study successfully demonstrates the synthesis and application of a novel Cu-Al/Biochar@g-C_3N_4 composite as an effective catalyst for the Fenton-based degradation of quinoline yellow (E104) dye. Comprehensive physicochemical characterization confirmed the successful doping of copper and aluminum onto the graphitic carbon nitride-modified biochar matrix, resulting in enhanced surface area and active sites crucial for catalytic activity. Systematic optimization via Response Surface Methodology identified optimal operational parameters (pH 5, 100 mg/L dye, 50 mg catalyst, 65 mmol/L H_2O_2), achieving a high degradation efficiency of 92.33% within 150 minutes. The process kinetics were best described by a pseudo-second-order model, indicating a chemisorption-influenced degradation mechanism. Furthermore, the catalyst maintained significant activity over three consecutive reuse cycles, underscoring its practical potential and relative stability. By utilizing waste-derived biochar, this work aligns with circular economy principles, offering a cost-effective and sustainable strategy for treating toxic dye-laden wastewater. Future research should focus on enhancing the long-term stability and reusability of the composite, evaluating its performance in real industrial effluents, and exploring the mechanistic pathways of radical generation and pollutant mineralization to facilitate full-scale environmental application.

Declaration of competing interest

The authors affirm that this study was conducted without any influence from financial conflicts or personal affiliations that could affect the findings.

Data availability

On request, data will be made available by corresponding author (A. Hosseini-Bandegharaei).

Funding

This work was financially supported by Semnan University, Semnan (12521/2023).

The use of generative AI and disclosure

The authors declare that the free version of ChatGPT was used during the preparation of this manuscript solely to improve language clarity and enhance readability. All content was subsequently reviewed and edited by the authors to ensure accuracy, and the authors take full responsibility for the final published version.

Reference

[1] Dükkancı, M., Gündüz, G., Yılmaz, S., & Prihod'ko, R. (2010). Heterogeneous Fenton-like degradation of Rhodamine 6G in water using CuFeZSM-5 zeolite catalyst prepared by hydrothermal synthesis. *Journal of hazardous materials*, *181*(1-3), 343-350.doi. 10.1016/j.jhazmat.2010.05.016

[2] Stolyarova, I. V., Kovban', I. B., Prikhod'ko, R. V., Kushko, A. O., Sychev, M. V., & Goncharuk, V. V. (2007). Relationship between the catalytic behavior of FeZSM-5 zeolites in oxidative degradation of dyes and the nature of their active centers. *Russian Journal of Applied Chemistry*, *80*(5), 746-753.doi.10.1134/S1070427207050114

[3] Bopda, A., Mafo, S. G. M., Ndongmo, J. N., Kenda, G. T., Fotsop, C. G., Kuete, I. H. T., ... & Anagho, S. G. (2022). Ferromagnetic biochar prepared from hydrothermally modified calcined mango seeds for Fenton-like degradation of indigo carmine. *C*, *8*(4), 81.

[4] Kaykhaii, M., Sasani, M., & Marghzari, S. (2018). Removal of dyes from the environment by adsorption process. *Chem. Mater. Eng*, *6*(2), 31-35. doi.10.13189/cme.2018.060201

[5] Bousalah, D., Zazoua, H., Boudjemaa, A., Benmounah, A., Messaoud-Boureghda, M. Z., & Bachari, K. (2022). Enhanced reactivity of the CuO-Fe2O3 intimate heterojunction for the oxidation of quinoline yellow dye (E104). *Environmental Science and Pollution Research*, *29*(46), 69988-69999.

[6] Chelghoum, H., Nasrallah, N., Tahraoui, H., Seleiman, M. F., Bouhenna, M. M., Belmeskine, H., ... & Amrane, A. (2024). Eco-friendly synthesis of ZnO nanoparticles for quinoline dye photodegradation and antibacterial applications using advanced machine learning models. *Catalysts*, *14*(11), 831. doi. 10.3390/catal14110831

[7] Foko, R. U. N., Fotsop, C. G., Tchuifon, D. R. T., Banenzoué, C., & Azebaze, A. G. B. (2025). Green synthesis of magnetic type Zeolites 4A as catalyst for the elimination of quinoline yellow by the Fenton process: Optimization

and kinetic investigation. *Hybrid Advances*, *9*, 100401. doi.10.1016/j.hybadv.2025.100401

[8] Amchova, P., Kotolova, H., & Ruda-Kucerova, J. (2015). Health safety issues of synthetic food colorants. *Regulatory toxicology and pharmacology*, *73*(3), 914-922.https://doi.org/10.1016/j.yrtph.2015.09.026

[9] Su, Y., Wu, Z., Wu, Y., Yu, J., Sun, L., & Lin, C. (2015). Acid Orange II degradation through a heterogeneous Fenton-like reaction using Fe–TiO_2 nanotube arrays as a photocatalyst. *Journal of Materials Chemistry A*, *3*(16), 8537-8544. https://doi.org/10.1039/C5TA00839E

[10] Zaviska, F., Drogui, P., Mercier, G., & Blais, J. F. (2009). Procédés d'oxydation avancée dans le traitement des eaux et des effluents industriels: Application à la dégradation des polluants réfractaires. *Revue des sciences de l'eau*, *22*(4), 535-564. doi.10.7202/038330ar

[11] Ahmed, H. R., Kayani, K. F., Ealias, A. M., & Aziz, K. H. H. (2025). A comprehensive review of forty adsorption isotherm models: an in-depth analysis of ten statistical error measures. *Water, Air, & Soil Pollution*, *236*(6), 346.https://doi.org/10.1007/s11270-025-07982-4

[12] Ahmed, H. R., & Kayani, K. F. (2024). A comparative review of Fenton-like processes and advanced oxidation processes for Methylene Blue degradation. *Inorganic Chemistry Communications*, *170*, 113467. https://doi.org/10.1016/j.inoche.2024.113467

[13] Babuponnusami, A., & Muthukumar, K. (2014). A review on Fenton and improvements to the Fenton process for wastewater treatment. *Journal of Environmental Chemical Engineering*, *2*(1), 557-572. doi.10.1016/j.jece.2013.10.011

[14] Mafo, S. G. M., Tchuifon, D. R. T., Ngakou, C. S., Fotsop, C. G., Kouteu, P. A. N., Doungmo, G., ... & Anagho, S. G. (2023). Study of the degradation of Bezaktiv Brilliant Blue by the Fenton process using a prepared ferromagnetic activated carbon from rubber seed hull as heterogeneous catalyst. *Desalination and Water Treatment*, *287*, 200-213.doi.10.5004/dwt.2023.29358

[15] Garrido-Ramírez, E. G., Theng, B. K., & Mora, M. L. (2010). Clays and oxide minerals as catalysts and nanocatalysts in Fenton-like reactions—a review. *Applied Clay Science*, *47*(3-4), 182-192.doi.org/10.1016/j.clay.2009.11.044

[16] Liu, Z., Zhang, Y., Lee, J., & Xing, L. (2024). A review of application mechanism and research progress of Fe/montmorillonite-based catalysts in heterogeneous Fenton reactions. *Journal of environmental chemical engineering*, *12*(2), 112152. doi.org/10.1016/j.jece.2024.112152

[17] Nyankson, E., Adjasoo, J., Efavi, J. K., Amedalor, R., Yaya, A., Manu, G. P., ... & Amartey, N. A. (2019). Characterization and evaluation of zeolite A/Fe3O4 nanocomposite as a potential adsorbent for removal of organic molecules from wastewater. *Journal of Chemistry*, *2019*(1), 8090756.

[18] Djioko, F. H. K., Fotsop, C. G., Youbi, G. K., Nwanonenyi, S. C., Oguzie, E. E., & Madu, C. A. (2024). Efficient removal of pharmaceutical contaminant in wastewater using low-cost zeolite 4A derived from kaolin: Experimental and theoretical studies. *Materials Chemistry and Physics*, *315*,

128994.doi. 10.1016/j.matchemphys.2024.128994
[19] Nguyen, M. V., & Lee, B. K. (2016). A novel removal of CO2 using nitrogen doped biochar beads as a green adsorbent. *Process Safety and Environmental Protection*, *104*, 490-498. doi.10.1016/j.psep.2016.04.007
[20] Ahmed, H. R. (2025). Heterogeneous catalysts in advanced oxidation processes : A comprehensive review on antibiotic removal from wastewater. Separation and Purification Technology, 374(May), 133670. https://doi.org/10.1016/j.seppur.2025.133670
[21] Ayuketah, Y., Gyamfi, S., Diawuo, F. A., & Dagoumas, A. S. (2023). Assessment of low-carbon energy transitions policies for the energy demand sector of Cameroon. *Energy for Sustainable Development*, *72*, 252-264. https://doi.org/10.1016/j.esd.2022.12.014
[22] Ahmed, H. R., Chawraba, K., Ealias, A. M., Kayani, K. F., & Hussain, A. (2026). Biocatalytic and enzymatic systems for heavy metal removal from aquatic environments: mechanisms, applications, and future prospects. *Environmental Geochemistry and Health*, *48*(3), 128.https://doi.org/10.1007/s10653-026-03027-9
[23] Amangelsin, Y., Semenova, Y., Dadar, M., Aljofan, M., & Bjørklund, G. (2023). The impact of tetracycline pollution on the aquatic environment and removal strategies. *Antibiotics*, *12*(3), 440. doi. 10.3390/antibiotics12030440
[24] Qu, J., Peng, W., Wang, M., Cui, K., Zhang, J., Bi, F., ... & Zhang, Y. (2024). Metal-doped biochar for selective recovery and reuse of phosphate from water: Modification design, removal mechanism, and reutilization strategy. *Bioresource Technology*, *407*, 131075. doi.10.1016/j.biortech.2024.131075
[25] Chemerys, V., & Baltrėnaitė, E. (2018). A review of lignocellulosic biochar modification towards enhanced biochar selectivity and adsorption capacity of potentially toxic elements. *Ukrainian Journal of Ecology*, *8*(1), 21-32.
[26] Gao, Y., Gao, W., Zhu, H., Chen, H., Yan, S., Zhao, M., ... & Zhang, S. (2022). A review on N-doped biochar for oxidative degradation of organic contaminants in wastewater by persulfate activation. *International Journal of Environmental Research and Public Health*, *19*(22), 14805.
[27] Marques, I. S., Jarrais, B., Ramos, R., Abdelkader-Fernandez, V. K., Yaremchenko, A., Freire, C., ... & Peixoto, A. F. (2023). Nitrogen-doped biochar-supported metal catalysts: High efficiency in both catalytic transfer hydrogenation of furfural and electrocatalytic oxygen reactions. *Catalysis Today*, *418*, 114080.doi.10.1016/j.cattod.2023.114080
[28] Tchuifon Tchuifon, D. R., Fotsop, C. G., Kenda, G. T., Feudjio, F. D. S., Mafo, S. G. M., Dongmo, D. S. M., ... & Hosseini-Bandegharaei, A. (2025). Efficient removal of tetracycline and norfloxacin contaminants in wastewater onto N-dopped Cu/Al@ Biochar as low-cost sorbent: kinetic and adsorption mechanism investigation. *Environmental Science and Pollution Research*, *32*(23), 14066-14085. doi.10.1007/s11356-025-36517-x
[29] Askari, H., Ghaedi, M., Dashtian, K., & Azghandi, M. H. A. (2017). Rapid and high-capacity ultrasonic assisted adsorption of ternary toxic anionic dyes onto MOF-5-activated carbon: artificial neural networks, partial least squares, desirability function and isotherm and kinetic

study. *Ultrasonics sonochemistry*, *37*, 71-82. doi.org/10.1016/j.ultsonch.2016.10.029

[30] Azad, F. N., Ghaedi, M., Dashtian, K., Hajati, S., & Pezeshkpour, V. (2016). Ultrasonically assisted hydrothermal synthesis of activated carbon–HKUST-1-MOF hybrid for efficient simultaneous ultrasound-assisted removal of ternary organic dyes and antibacterial investigation: Taguchi optimization. *Ultrasonics sonochemistry*, *31*, 383-393. doi. 10.1016/j.ultsonch.2016.01.024

[31] Karimi, R., Yousefi, F., Ghaedi, M., & Rezaee, Z. (2019). Comparison the behavior of ZnO–NP–AC and Na, K doped ZnO–NP–AC for simultaneous removal of Crystal Violet and Quinoline Yellow dyes: Modeling and optimization. *Polyhedron*, *170*, 60-69.doi. 10.1016/j.poly.2019.05.038

[32] Heidari, M., Vosoughi, M., Sadeghi, H., Dargahi, A., & Mokhtari, S. A. (2021). Degradation of diazinon from aqueous solutions by electro-Fenton process: effect of operating parameters, intermediate identification, degradation pathway, and optimization using response surface methodology (RSM). *Separation Science and Technology*, *56*(13), 2287-2299.doi. 10.1080/01496395.2020.1821060

[33] Dargahi, A., Samarghandi, M. R., Shabanloo, A., Mahmoudi, M. M., & Nasab, H. Z. (2023). Statistical modeling of phenolic compounds adsorption onto low-cost adsorbent prepared from aloe vera leaves wastes using CCD-RSM optimization: effect of parameters, isotherm, and kinetic studies. *Biomass Conversion and Biorefinery*, *13*(9), 7859-7873.

[34] Carvalho, A. P., Costa, J., Martins, A., Fonseca, A. M., Neves, I. C., & Nunes, N. (2025). Zeolite Modification for Optimizing Fenton Reaction in Methylene Blue Dye Degradation. *Colorants*, *4*(1), 10.

[35] Chen, B., Chen, Z., & Lv, S. (2011). A novel magnetic biochar efficiently sorbs organic pollutants and phosphate. *Bioresource technology*, *102*(2), 716-723. doi.10.1016/j.biortech.2010.08.067

[36] Avila, C., Pang, C. H., Wu, T., & Lester, E. (2011). Morphology and reactivity characteristics of char biomass particles. *Bioresource technology*, *102*(8), 5237-5243. doi. 10.1016/j.biortech.2011.01.071

[37] Lv, W., Liu, B., Qiu, Q., Wang, F., Luo, Z., Zhang, P., & Wei, S. (2009). Synthesis, characterization and photocatalytic properties of spinel CuAl2O4 nanoparticles by a sonochemical method. *Journal of alloys and compounds*, *479*(1-2), 480-483. doi.10.1016/j.jallcom.2008.12.111

[38] Allwar, A., Ahdiaty, R., & Doong, R. (2022). Magnetic Fe3O4-CuO/biochar nanocomposite for adsorption of inorganic anions from aqueous solution. *Rasayan J Chem*, *15*(4), 2466-2476.

[39] Liu, Y., Qing, S., Hou, X., Feng, G., Zhang, R., Wang, X., ... & Xiang, H. (2018). Synthesis and structural characterization of CuAl2O4 spinel with an unusual cation distribution. *Journal of Materials and Applications*, *7*(2), 82-89.

[40] Wabo, S. P., Nanssou Kouteu, P. A., Hzounda Fokou, J. B., Mbiada Pahane, M., Mouangue, R. M., & Jiokap Nono, Y. (2025). Optimisation of ultrasonic-assisted biosynthesis of silver nanoparticles mediated by Raphia farinifera kernel extract using neural network and Box-Behnken design for the catalytic degradation of organic dyes. *International Journal of Environmental Analytical Chemistry*, *105*(20), 9266-9289.

[41] Ahmed, H. R., & Karim, A. R. (2025). Structural insights into metal oxide nanocomposite graphene frameworks as catalysts for oxidative desulfurization of light gasoil. *Journal of Molecular Structure*, *1325*, 141081.of organic dyes. *International Journal of Environmental Analytical Chemistry*, *105*(20), 9266-9289.

[42] Liang, M., Li, X., Lin, Y., Zhang, K., & Lu, F. (2019). Dynamic compressive behaviors of two-layer graded aluminum foams under blast loading. *Materials*, *12*(9), 1445.

[43] Zhang, A., Li, X., Xing, J., & Xu, G. (2020). Adsorption of potentially toxic elements in water by modified biochar: A review. *Journal of Environmental Chemical Engineering*, *8*(4), 104196. doi.10.1016/j.jece.2020.104196

[44] Jin, M., Zhou, Q., Fu, L., & Wu, W. (2025). Application of biochar-based catalysts for soil and water pollution control. *Topics in Catalysis*, *68*(5), 591-614.

[45] Li, S., & Chen, G. (2018). Thermogravimetric, thermochemical, and infrared spectral characterization of feedstocks and biochar derived at different pyrolysis temperatures. *Waste Management*, *78*, 198-207. doi.10.1016/j.wasman.2018.05.048

[46] Mukhamed'yarova, A. N., Gareev, B. I., Nurgaliev, D. K., Aliev, F. A., & Vakhin, A. V. (2021). A review on the role of amorphous aluminum compounds in catalysis: avenues of investigation and potential application in petrochemistry and oil refining. *Processes*, *9*(10), 1811.

[47] Ahmad, M., Rajapaksha, A. U., Lim, J. E., Zhang, M., Bolan, N., Mohan, D., ... & Ok, Y. S. (2014). Biochar as a sorbent for contaminant management in soil and water: a review. *Chemosphere*, *99*, 19-33.doi.10.1016/j.chemosphere.2013.10.071

[48] Chen, B., & Yuan, M. (2011). Enhanced sorption of polycyclic aromatic hydrocarbons by soil amended with biochar. *Journal of Soils and Sediments*, *11*(1), 62-71.doi.10.1007/s11368-010-0266-7

[49] Li, Y., Shao, J., Wang, X., Deng, Y., Yang, H., & Chen, H. (2014). Characterization of modified biochars derived from bamboo pyrolysis and their utilization for target component (furfural) adsorption. *Energy & Fuels*, *28*(8), 5119-5127. doi.10.1021/ef500725c

[50] Baragh, F., El Bouadi, O., Draoui, K., El Bali, B., Agunaou, M., & Kherbeche, A. (2019). Comparative study on degradation of p-nitrophenol from aqueous solution by catalytic wet peroxide oxidation using pillared bentonite clay catalysts. *Desalination and Water Treatment*, *143*, 217-228. doi.10.5004/dwt.2019.23528

[51] Juturu, R., Vinayagam, R., Murugesan, G., & Selvaraj, R. (2025). Enhanced adsorptive removal of chromium (VI) ions from wastewater with phosphorus-doped magnetite-carbon composite: advanced statistical physics modeling and kinetic studies. *Environment, Development and Sustainability*, 1-27.

[52] Ferroudj, N., Talbot, D., Michel, A., Davidson, A., & Abramson, S. (2017). Increasing the efficiency of magnetic heterogeneous Fenton catalysts with a simple halogen visible lamp. *Journal of Photochemistry and Photobiology A: Chemistry*, *338*, 85-95.doi.10.1016/j.jphotochem.2017.01.029

[53] Chen, J., Liu, M., Zhang, L., Zhang, J., & Jin, L. (2003). Application of nano TiO2 towards polluted water treatment combined with electro-photochemical method. *Water research*, *37*(16), 3815-3820.

doi.10.1016/S0043-1354(03)00332-4
[54] Saritha, P., Aparna, C., Himabindu, V., & Anjaneyulu, Y. J. J. O. H. M. (2007). Comparison of various advanced oxidation processes for the degradation of 4-chloro-2 nitrophenol. *Journal of hazardous materials*, *149*(3), 609-614. doi.10.1016/j.jhazmat.2007.06.111
[55] Sawood, G. M., Mishra, A., & Gupta, S. K. (2021). Optimization of arsenate adsorption over aluminum-impregnated tea waste biochar using RSM–central composite design and adsorption mechanism. *Journal of Hazardous, Toxic, and Radioactive Waste*, *25*(2), 04020075. doi.10.1061/(asce)hz.2153-5515.0000581
[56] Palapa, N. R., Taher, T., Siregar, P. M. S. B. N., Juleanti, N., Wijaya, A., Badri, A. F., & Lesbani, A. (2021). High structural stability and adsorption capacity of Zn/Al-biochar and Cu/Al-biochar toward adsorption of Cr (VI). *Journal of Ecological Engineering*, *22*(4). doi.10.12911/22998993/134153
[57] Tsokeing, C. L., Dongmo, S. D. M., Maffeu, E. J., Tchieta, P. G., & Wansi, J. D. (2025). Study of the degradation of RY-145 b y the fenton process using a prepared magnetic bentonite as heterogeneous catalyst. *Hybrid Advances*, *10*, 100463.doi.10.1016/j.hybadv.2025.100463
[58] Zahedi, S., Asadipour, A., Dolatabadi, M., & Ahmadzadeh, S. (2022). Response surface modeling for the treatment of methylene blue from aqueous media using electro-Fenton process before determination by UV-VIS spectrometer: Kinetic and degradation mechanism. *Analytical Methods in Environmental Chemistry Journal*, *5*(02), 39-50.
[59] Juturu, R., Vinayagam, R., Murugesan, G., & Selvaraj, R. (2025). Mesoporous hydrochar from Acacia falcata leaves by hydrothermal process for hexavalent chromium adsorption. *Scientific Reports*, *15*(1), 12670.
[60] Silva, J. O., Granja, H. S., Santos, J. F. D., Freitas, L. S., & Sussuchi, E. M. (2024). Biochar and hydrochar in the development and application of electrochemical devices in the sensing and degradation of target compounds: A Mini-Review of the recent contributions of 2020-2023. *Journal of the Brazilian Chemical Society*, *35*(1), e-20230143.
[61] Juturu, R., Vinayagam, R., Murugesan, G., & Selvaraj, R. (2025). Synthesis and characterization of Zn and Fe doped magnetic biochar from Acacia falcata leaves for Cr (VI) adsorption. *Scientific Reports*, *15*(1), 22146.
[62] Chen, K., Wang, G. H., Li, W. B., Wan, D., Hu, Q., & Lu, L. L. (2014). Application of response surface methodology for optimization of Orange II removal by heterogeneous Fenton-like process using Fe3O4 nanoparticles. *Chinese Chemical Letters*, *25*(11), 1455-1460.doi.10.1016/j.cclet.2014.06.014